Energy Transfer

DOI: 10.1002/anie.201205082

Perfluorinated Aromatic Spacers for Sensitizing Europium(III) Centers in Dinuclear Oligomers: Better than the Best by Chemical Design?**

Jean-François Lemonnier, Lucille Babel, Laure Guénée, Prasun Mukherjee, David H. Waldeck, Svetlana V. Eliseeva, Stéphane Petoud,* and Claude Piguet**

The unique optical characteristics of lanthanide ions (Ln^{III}) have driven their use in a wide range of applications; however, the efficiency of populating their electronic states directly is limited, and thus there is a great need to create an antenna to capture energy and generate excited Ln^{III} ions. In this context, metal–organic frameworks, hybrid materials, and nanoparticles randomly doped with homo- or heterometallic mixtures of luminescent lanthanide cations (Ln^{III}) are intensively being investigated for engineering luminescent devices for bright-white lighting, for upconversion, and as sensing agents.[1] Although the exact location of the various metals in the final material is crucial for dual ligand-centered/metal-centered emission,[1l,m] for upconversion,[1g] and for directional light-conversion[2a] processes, the preparation of organized polymetallic 4f-4f oligomers and polymers remains rare and challenging.[2] A statistical mechanics (Ising model) analysis suggests that standard repulsive nearest neighbor intermetallic interactions operating in linear polymers with regularly spaced binding sites should provide the targeted ordered …-Ln^1-Ln^2-Ln^1-Ln^2-… microstates.[3,4] Pioneering work in this field has relied on the bulk electropolymerization of didentate 1,10-phenanthroline with thienyl spacers,[5] and the acyclic diene metathesis of tridentate 2,6-bis(benzimidazol-2-yl)pyridine,[6] followed by reaction with [Eu(β-diketonate)$_3$] or $Eu(NO_3)_3$ to yield red-emitting metallopolymers. A reliable exploitation of this concept for the development of luminescent materials, however, requires the efficient sensitization of the luminophore through the rational optimization of each photophysical step by using chemical tools.

As a first step toward this goal, the rigid segmental ligand strands **L1**–**L3**, made of two tridentate binding units separated by a rigid and electronically tunable aromatic spacer, have been treated with trivalent europium to give the dinuclear complexes [Eu_2(**L**)(hfac)$_6$] (Scheme 1; hfac = hexafluoroacetonato).[7] The use of a simple method for deciphering the various contributions to the sensitization mechanism clearly showed that [Eu_2(**L3**)(hfac)$_6$] had the largest global emission quantum yield [$\Phi_{Eu}^{L} = 0.206(7)$, Eqs. (1) and (2)] because of an efficient **L3**→Eu energy transfer step [$\eta_{en.tr.}^{L\rightarrow Eu} = 0.47(14)$; Eq. (3), see the dark gray bars in Figure 1].[7]

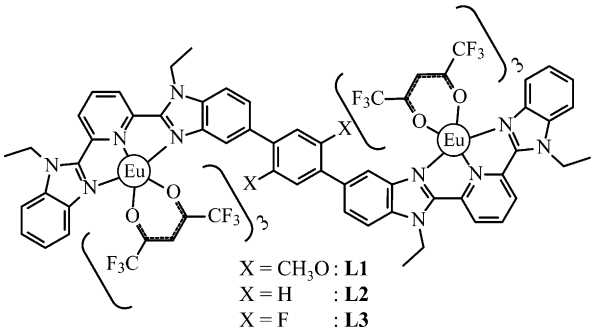

Scheme 1. Chemical structures of complexes [Eu_2(**L**)(hfac)$_6$].

$$\Phi_{Eu}^{L} = \eta_{ISC}\eta_{en.tr.}^{L\rightarrow Eu}\Phi_{Eu}^{Eu} \quad (1)$$

$$\eta_{ISC} = \frac{k_{ISC}}{k_r^F + k_{nr}^F + k_{ISC}} \quad (2)$$

$$\eta_{en.tr.}^{L\rightarrow Eu} = \frac{2k_{en.tr.}^{Eu}}{k_r^P + k_{nr}^P + k_{en.tr.}^{Eu}} = 2k_{en.tr.}^{Eu}\tau_L^{Eu}({}^3\pi^*) \quad (3)$$

Theoretical considerations suggest that $\eta_{en.tr.}^{L\rightarrow Eu}$ could benefit from a shift of the **L**($^3\pi^*$) state to higher energy through perfluorination of the central aromatic spacer to give **L4** (Scheme 2).[8] Correspondingly, the expected decrease in the k_{nr}^F and k_{nr}^{Eu} values, and of the so-called π-conjugation length A_π [Eq. (5)][9] in [Eu_2(**L4**)(hfac)$_6$],[7] should optimize both the intersystem crossing efficiency [η_{ISC} =0.6(1), Eq. (2)] and the intrinsic Eu-centered quantum yield [Φ_{Eu}^{Eu} =0.76(2), Eq. (4)] of those previously measured for [Eu_2(**L3**)(hfac)$_6$] (dark gray bars in Figure 1).

[*] Dr. J.-F. Lemonnier, L. Babel, Prof. Dr. C. Piguet
Department of Inorganic Analytical Chemistry
University of Geneva
30 quai E. Ansermet, CH-1211 Geneva 4 (Switzerland)
E-mail: claude.piguet@unige.ch
Dr. L. Guénée
Laboratory of Crystallography, University of Geneva
24 quai E. Ansermet, CH-1211 Geneva 4 (Switzerland)
Dr. P. Mukherjee, Prof. Dr. D. H. Waldeck
Department of Chemistry, University of Pittsburgh
219 Parkman Avenue, Pittsburgh, PA 15260 (USA)
E-mail: dave@pitt.edu
Dr. S. V. Eliseeva, Prof. Dr. S. Petoud
Centre de Biophysique Moléculaire
CNRS UPR 4301, Rue Charles Sadron
F-45071 Orléans Cedex 2 (France)
E-mail: stephane.petoud@cnrs-orleans.fr

[**] This work was supported through grants from the Swiss National Science Foundation, the National Institutes of Health (through NIH grant R21-EB008257-01A1), the National Science Foundation (CHE-0718755), as well as la Ligue contre le Cancer and the Institut National de la Santé et de la Recherche Médicale (INSERM). The work was carried out within the COST Actions D38 and CM1006.
Supporting information for this article is available on the WWW under http://dx.doi.org/10.1002/anie.201205082.

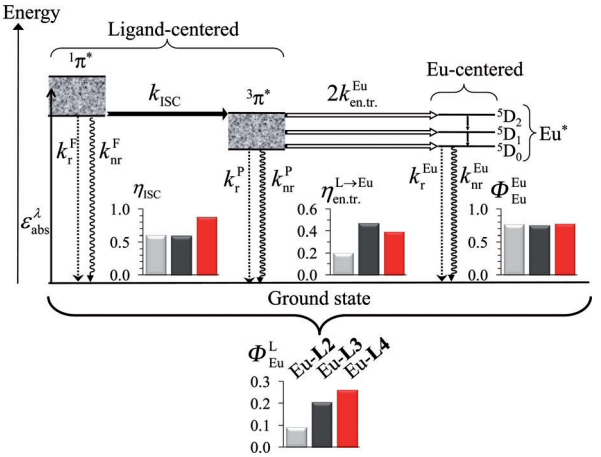

Figure 1. Simplified Jablonski diagram for $[Eu_2(\mathbf{L})(hfac)_6]$ (**L** = **L2**–**L4**) showing the ligand-centered triplet-mediated sensitization mechanism of the two Eu^{3+} ions.[10] The photophysical processes are described by the rate constants: k_r^F for the ligand fluorescence, k_{nr}^F for the internal nonradiative conversion of the ligand, k_r^P for the ligand phosphorescence, k_{nr}^P for nonradiative relaxation from the ligand triplet state, k_r^{Eu} for the emission of Eu^*, k_{nr}^{Eu} for the nonradiative decay of Eu^*, k_{ISC} for ligand intersystem crossing, and $k_{en.tr.}^{Eu}$ for the ligand-to-metal energy transfer. The efficiencies of intersystem crossing (η_{ISC}), energy transfer ($\eta_{en.tr.}^{L\rightarrow Eu}$), intrinsic quantum yield (Φ_{Eu}^{Eu}), and quantum yield (Φ_{Eu}^{L}) for the global ligand-mediated sensitization of Eu^{III} in $[Eu_2(\mathbf{L})(hfac)_6]$ (solid-state, 293 K) are also shown.

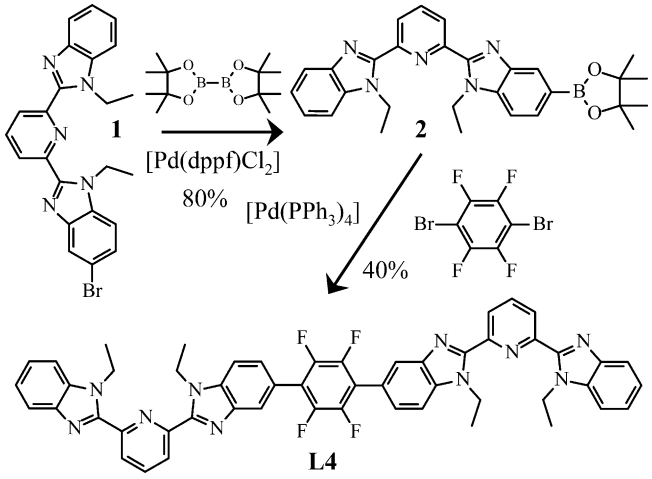

Scheme 2. Synthesis of the perfluorinated ligand **L4**.

$$\Phi_{Eu}^{Eu} = \frac{k_r^{Eu}}{k_r^{Eu} + k_{nr}^{Eu}} = k_r^{Eu} \cdot \tau_{Eu} \quad (4)$$

$$k_r^F = k_{nr}^F \cdot e^{A_\alpha} \quad (5)$$

The centrosymmetrical perfluorinated ligand **L4** is obtained through two successive palladium-catalyzed Suzuki–Myaura cross-coupling reactions (Scheme 2; see also Figures S1 and S2 in the Supporting Information). Mixing stoichiometric amounts of **L4** with [Ln(hfac)$_3$(diglyme)] (2.0 equiv) in chloroform gives $[Ln_2(\mathbf{L4})(hfac)_6]$ (Ln = Gd, Eu) in 80% yield. Slow evaporation of concentrated acetonitrile/chloroform solutions containing the europium complex, provided X-ray quality prisms (see Table S1 in the Supporting Information) including S-shaped centrosymmetrical neutral $[Eu_2(\mathbf{L4})(hfac)_6]$ complexes, in which the Eu atoms are separated by 14.667(1) Å (Figure 2). Each metal

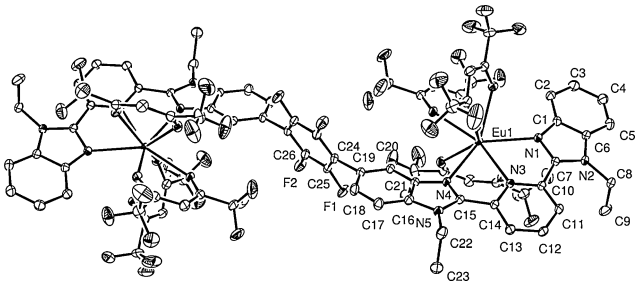

Figure 2. Perspective view of the molecular structure and numbering scheme of $[Eu_2(\mathbf{L4})(hfac)_6]$, as obtained from X-ray diffraction. Thermal ellipsoids are represented at the 30% probability level and hydrogen atoms are omitted for clarity.

center is nine-coordinate in a highly distorted monocapped square antiprismatic polyhedron, produced by the three nitrogen atoms of the bound tridentate aromatic unit and by the six oxygen atoms of the three didentate hexafluoroacetylacetonate moieties, with N1 occupying the capping position (see the Supporting Information). All the bond distances and bond angles are standard (see Tables S2–S4 in the Supporting Information) and the solid-state molecular structures of $[Yb_2(\mathbf{L3})(hfac)_6]$ and $[Eu_2(\mathbf{L4})(hfac)_6]$ are almost superimposable, except for the interannular phenyl–benzimidazole twist angle, which increases from 54.1(1)° to 66.2(1)° (see Figure S3 and Table S5 in the Supporting Information).

Irradiation into the allowed ligand-centered $^1\pi^* \leftarrow {}^1\pi$ transition of $[Eu_2(\mathbf{L4})(hfac)_6]$ at $\bar{\nu}_{exc} = 28\,170\ cm^{-1}$ produces an intense long-lived red emission signal arising from **L4**$\rightarrow Eu^{III}$ energy transfer followed by an Eu($^5D_1$)- and Eu($^5D_0$)-centered luminescence (see Figure S4 in the Supporting Information). The emission spectrum is dominated by the hypersensitive forced electric dipolar Eu($^5D_0 \rightarrow {}^7F_2$) transition centered at 16340 cm^{-1}, which leads to the largest global absolute quantum yields in this series (Φ_{Eu}^{L} = 0.26(1), solid state, 293 K; Table 1, entry 6).[11] Using Einstein's result for the spontaneous radiative emission rate,[12] the radiative rate constant k_r^{Eu} Table 1, entry 2) is deduced from the I_{tot}/I_{MD} ratio, where I_{tot} is the integrated emission for the Eu($^5D_0$) level ($^5D_0 \rightarrow {}^7F_J$, J = 0–4) and I_{MD} is the integrated intensity of the magnetic dipolar Eu($^5D_0 \rightarrow {}^7F_1$) transition (Table 1, entry 1). In combination with the characteristic lifetime τ_{Eu} = 0.90(1) ms (Table 1, entry 3), we calculate Φ_{Eu}^{Eu} = 0.77(1) for the intrinsic Eu-centered quantum yield [Eq. (4); Table 1, entry 4], a value identical to that obtained for $[Eu_2(\mathbf{L3})(hfac)_6]$. This finding implies that the gain in global quantum yields can be assigned specifically to the improved sensitization process $\eta_{sens} = \eta_{ISC}\eta_{en.tr.}^{L\rightarrow Eu} = \Phi_{Eu}^{L}/\Phi_{Eu}^{Eu}$ = 0.34(1) operating in $[Eu_2(\mathbf{L4})(hfac)_6]$ [Eq. (1); Table 1, entry 7). Given that the experimental ligand-centered fluorescence lifetimes measured for the $[Gd_2(\mathbf{L})(hfac)_6]$ complexes (**L** = **L1**–**L4**, Table S6) are only

Table 1: Experimental global (Φ_{Eu}^{L}) and intrinsic (Φ_{Eu}^{Eu}) quantum yields, luminescence lifetimes (τ_{Eu}) as well as calculated energy migration efficiencies (η_{ISC}, $\eta_{en.tr.}^{L\to Eu}$) and rate constants (k_r^{Eu}, k_{nr}^{Eu}, $k_{en.tr.}^{Eu}$, k_r^P, k_{nr}^P, k_{ISC}) for $[Eu_2(\mathbf{L})(hfac)_6]$ in the solid state at 293 K ($k = 2$–4).[10]

Compound	$[Eu_2(\mathbf{L2})(hfac)_6]$	$[Eu_2(\mathbf{L3})(hfac)_6]$	$[Eu_2(\mathbf{L4})(hfac)_6]$
Eu-centered luminescence			
I_{tot}/I_{MD}	17.5(3)	18.2(3)	17.2(2)
I_{tot}/I_{MD} [ms^{-1}]	0.86(2)	0.90(2)	0.85(1)
k_r^{Eu} [ms]	0.88(4)	0.83(15)	0.90(1)
Φ_{Eu}^{Eu}	0.76(4)	0.75(1)	0.77(1)
k_{nr}^{Eu} [ms^{-1}]	0.21(1)	0.23(4)	0.200(4)
global quantum yield and sensitization efficiency			
Φ_{Eu}^{L}	0.092(3)	0.206(7)	0.26(1)
$\eta_{ISC}\eta_{en.tr.}^{L\to Eu}$	0.122(7)	0.28(5)	0.34(1)
energy migration and associated rate constants			
k_{ISC}^{Gd-L} [ns^{-1}]	10.0(6)	9(2)	30(4)
$k_r^F + k_{nr}^F$ [ns^{-1}]	6.71(5)	6.25(3)	4.00(5)
η_{ISC}	0.60(3)	0.59(12)	0.88(15)
$\eta_{en.tr.}^{L\to Eu}$	0.20(2)	0.47(14)	0.39(6)
$2k_{en.tr.}^{Eu}$ [ms^{-1}]	2.1(3)	5.5(2.3)	5.7(2.1)
$k_r^P + k_{nr}^P$ [ms^{-1}]	8.1(5)	6.3(8)	9.1(2.5)
reference	[7]	[7]	this work

30–60 ps, one can assume that the energy migration processes in $[Eu_2(\mathbf{L})(hfac)_6]$ are described well by the exclusive contribution of the triplet state, as shown in Figure 1.[7,13] Considering that 1) the sum of the radiative and internal nonradiative conversion rate constants $k_r^F + k_{nr}^F$ controlling the relaxation of the $^1\pi^*$ excited state in the free ligand are the same in the gadolinium complex $[Gd_2(\mathbf{L4})(hfac)_6]$ and that 2) $k_{ISC}^{\mathbf{L4}} \ll k_{ISC}^{Gd-\mathbf{L4}}$, because of the paramagnetic and heavy atom effects generated by the Gd^{III} center,[14] the introduction of the experimental characteristic lifetimes of $^1\pi^*$ measured in **L4** ($\tau_L^{\mathbf{L4}}(^1\pi^*) = 0.25(2)$ ns) and in $[Gd_2(\mathbf{L4})(hfac)_6]$ ($\tau_L^{Gd-\mathbf{L4}}(^1\pi^*) = 0.029(6)$ ns; see also Table S6 in the Supporting Information) into Equation (6) gives $k_{ISC}^{Gd-\mathbf{L4}} = 30(4)$ ns^{-1}

$$\frac{1}{\tau_L^{Gd-\mathbf{L}}(^1\pi^*)} - \frac{1}{\tau_L^{\mathbf{L}}(^1\pi^*)} = \left(k_r^F + k_{nr}^F + k_{ISC}^{Gd-\mathbf{L}}\right) - \left(k_r^F + k_{nr}^F + k_{ISC}^{\mathbf{L}}\right) = k_{ISC}^{\mathbf{L}} - k_{ISC}^{Gd-\mathbf{L}} \approx k_{ISC}^{Gd-\mathbf{L}} \quad (6)$$

(Table 1, entry 8) and $k_r^F + k_{nr}^F = 4.00(5)$ ns^{-1} (Table 1, entry 9), from which $\eta_{ISC} = 0.88(15)$ can be deduced with Equation (2) (Table 1, entry 10).[7]

Finally, the energy transfer efficiency $\eta_{en.tr.}^{L\to Eu} = \eta_{sens}/\eta_{ISC} = 0.39(6)$ and the associated rate constant $2k_{en.tr.}^{Eu} = \left[\eta_{en.tr.}^{L\to Eu}/\left(1-\eta_{en.tr.}^{L\to Eu}\right)\right]\left(k_r^P + k_{nr}^P\right) = 5.7(2.1)$ ms^{-1} [Eq. (3), with $\left(k_r^P + k_{nr}^P\right) = 1/\tau_L^{Gd-\mathbf{L4}}(^3\pi^*) = 9.1(2.5)$ ms^{-1}] calculated for $[Eu_2(\mathbf{L4})(hfac)_6]$ (Table 1, entries 11 and 12) indicates no noticeable improvement in these parameters on changing from the difluorinated (**L3**) to the perfluorinated (**L4**) spacer, despite the 500–1000 cm^{-1} blue shift of the ligand-centered $^1\pi^*$ (Figure S5 in the Supporting Information) and $^3\pi^*$ (Figure S6 in the Supporting Information) excited states. Our simple method for dissecting the sensitization mechanism[7] shows that the gain in the global quantum yield Φ_{Eu}^{L} for the complex $[Eu_2(\mathbf{L4})(hfac)_6]$ compared to $[Eu_2(\mathbf{L3})(hfac)_6]$ indeed results from an optimization of the intersystem crossing process η_{ISC} (Figure 1).

Scrutiny of the various rate constants (Table 1 and see Table S7 in the Supporting Information) reveals that the decrease in the radiative and internal conversion rate constants $k_r^F + k_{nr}^F$ for the ligand-centered $\mathbf{L}(^1\pi^*)$ state along the series **L2** > **L3** > **L4** acts to improve η_{ISC} [Eq. (2)], but it is the remarkable increase in $k_{ISC}^{Ln-\mathbf{L}}$ of $[Ln_2(\mathbf{L4})(hfac)_6]$ which eventually controls the overall intersystem crossing efficiency.

The physical origin of this beneficial effect can be traced back to the golden-rule expression for radiationless transitions [Eq. (7)]:[15]

$$k_{ISC} = \frac{2\pi}{\hbar}\langle ^1\pi^*|H_{SO}|^3\pi^*\rangle^2 \mathrm{FCWDS} \quad (7)$$

where FCWDS is the Franck–Condon weighted density of states. It accounts for the density of vibrational states in the triplet state and their vibrational overlap with the singlet vibrational state. A model that accounts for the thermal population of levels and uses a single quantum mode of frequency ω is commonly associated with the Marcus–Levich–Jortner theory for electron transfer [Eq. (8)]:[16]

$$\mathrm{FCWDS} = \frac{\exp(-S)}{\sqrt{4\pi RT}}\sum_{n=0}^{\infty}\frac{S^n}{n!}\exp\left[-\frac{(\Delta E + n\hbar\omega + \lambda)}{4\lambda RT}\right] \quad (8)$$

The spin–orbit coupling matrix element $\langle ^1\pi^*|H_{SO}|^3\pi^*\rangle$ reaches a maximum for nonplanar polyaromatic molecules containing heavy paramagnetic atoms in the molecular frame;[16,17] two conditions which are fulfilled by all the $[Eu_2(\mathbf{L})(hfac)_6]$ complexes described in this study. We note, however, that the deviation from planarity, as measured by the interplanar phenyl–benzimidazole angles, increases along the series **L2** (25.26(4)°) < **L3** (54.1(1)°) < **L4** (66.2(1)°), in line with the k_{ISC} values [Eq. (7) and Table 1). The Franck–Condon weighted density of states (FCWDS) depends on the singlet–triplet energy splitting $\Delta E = E(^1\pi^*) - E(^3\pi^*)$ and on the reorganization energy λ, which corresponds to the energy difference between the triplet and the singlet state at its equilibrium geometry [Eq. (8)].[18] Within the limitation of parabolic surfaces, this energy parameter, along with the ΔE value, provides the energy gap for $n = 0$. The successive fluorination of the ligands along the series $[Eu_2(\mathbf{L})(hfac)_6]$ (**L2**–**L4**) is known to significantly affect the frontier orbitals, and hence the λ as well as ΔE and FCWDS values in Equation (8).[7] While a quantitative understanding of the changes in λ requires sophisticated theoretical calculations of the vibrational coupling scheme controlling the Huang–Rhys factors (S),[15,16] Equations (7) and (8) predict that the increasing ligand-centered energy gap ΔE observed along the series **L2** (3550 cm^{-1}) ≈ **L3** (3230 cm^{-1}) < **L4** (5200 cm^{-1}) should lower the k_{ISC} and η_{ISC} values. The apparent contradiction with our experimental results (Table 1, entries 8 and 10) can be resolved by including higher lying triplet states $^3\pi_{n>1}^*$ in the model, an approach used successfully for oligothiophenes[15] and helicenes.[15b] This counterintuitive correlation was noticed empirically for other polyaromatic chromophores, and it was suggested as a "rule-of-thumb" that a singlet–triplet gap of $E(^1\pi^*) - E(^3\pi^*) \geq 5000$ cm^{-1} warrants inclusion of quantitative intersystem crossing processes in Tb

and Eu complexes.[19] Given that the singlet–triplet energy gap can be readily calculated by using DFT[7] or semiempirical[8] methods, computations may be useful for identifying simple chemical and structural modifications that will enhance the quantum efficiency further.

In conclusion, the application of this simple method for analyzing the various contributions to the sensitization of Eu^{III} luminescence shows that perfluorination of the remote phenyl spacer in the rigid single-stranded dumbbell-shaped $[Eu_2(\mathbf{L4})(hfac)_6]$ oligomer optimizes both intersystem crossing efficiency and the intrinsic Eu^{III} quantum yield, thus maximizing the global quantum yields in these polyaromatic rigid complexes (red bars in Figure 1).

Received: June 28, 2012
Published online: October 9, 2012

Keywords: energy conversion · fluorinated ligands · intersystem crossing · lanthanides · ligand effects

[1] a) J. Kido, Y. Okamoto, *Chem. Rev.* **2002**, *102*, 2357–2368; b) R. C. Evans, P. Douglas, C. J. Winscom, *Coord. Chem. Rev.* **2006**, *250*, 2093–2126; c) A. de Bettencourt-Dias, *Dalton Trans.* **2007**, 2229–2241; d) K. Binnemans, *Chem. Rev.* **2009**, *109*, 4283–4374; e) N. Kerbellec, D. Kustaryono, V. Haquin, M. Etienne, C. Daiguebonne, O. Guillou, *Inorg. Chem.* **2009**, *48*, 2837–2843; f) G.-L. Law, K.-L. Wong, H.-L. Tam, K.-W. Cheah, W.-T. Wong, *Inorg. Chem.* **2009**, *48*, 10492–10494; g) K. Zheng, D. Zhang, D. Zhao, N. Liu, F. Shi, W. Qin, *Phys. Chem. Chem. Phys.* **2010**, *12*, 7620–7625; h) M. A. Katkova, M. N. Bochkarev, *Dalton Trans.* **2010**, *39*, 6599–6612; i) S. V. Eliseeva, J.-C. G. Bünzli, *Chem. Soc. Rev.* **2010**, *39*, 189–227; j) G. M. Farinola, R. Ragni, *Chem. Soc. Rev.* **2011**, *40*, 3467–3482; k) Y. Cui, Y. Yue, G. Qian, B. Chen, *Chem. Rev.* **2012**, *112*, 1126–1162; l) Y. Liu, M. Pan, Q.-Y. Yang, L. Fu, K. Li, S.-C. Wei, C.-Y. Su, *Chem. Mater.* **2012**, *24*, 1954–1960; m) D. F. Sava, L. E. S. Rohwer, M. A. Rodriguez, T. M. Nenoff, *J. Am. Chem. Soc.* **2012**, *134*, 3983–3986.

[2] a) J.-C. G. Bünzli, C. Piguet, *Chem. Rev.* **2002**, *102*, 1897–1928; b) C. M. G. dos Santos, A. J. Harte, S. J. Quinn, T. Gunnlaugsson, *Coord. Chem. Rev.* **2008**, *252*, 2512–2527; c) S. Swavey, R. Swavey, *Coord. Chem. Rev.* **2009**, *253*, 2627–2638; d) S. Faulkner, L. S. Natrajan, W. S. Perry, D. Sykes, *Dalton Trans.* **2009**, 3890–3899; e) P. A. Vigato, V. Peruzzo, S. Tamburini, *Coord. Chem. Rev.* **2009**, *253*, 1099–1201; f) C. Lincheneau, F. Stomeo, S. Comby, T. Gunnlaugsson, *Aust. J. Chem.* **2011**, *64*, 1315–1326.

[3] a) M. Borkovec, J. Hamacek, C. Piguet, *Dalton Trans.* **2004**, 4096–4105; b) C. Piguet, M. Borkovec, J. Hamacek, K. Zeckert, *Coord. Chem. Rev.* **2005**, *249*, 705–726.

[4] N. Dalla-Favera, J. Hamacek, M. Borkovec, D. Jeannerat, G. Ercolani, C. Piguet, *Inorg. Chem.* **2007**, *46*, 9312–9322.

[5] X.-Y. Chen, X. Yang, B. J. Holliday, *J. Am. Chem. Soc.* **2008**, *130*, 1546–1547.

[6] B. M. McKenzie, R. J. Wojtecki, K. A. Burke, C. Zhang, A. Jakli, P. T. Mather, S. J. Rowan, *Chem. Mater.* **2011**, *23*, 3525–3533.

[7] J.-F. Lemonnier, L. Guénée, C. Beuchat, T. A. Wesolowski, P. Mukherjee, D. H. Waldeck, K. A. Gogik, S. Petoud, C. Piguet, *J. Am. Chem. Soc.* **2011**, *133*, 16219–16234.

[8] R. O. Freire, R. Q. Albuquerque, S. A. Junior, G. B. Rocha, M. E. Mesquita, *Chem. Phys. Lett.* **2005**, *405*, 123–126.

[9] Y. Yamaguchi, Y. Matsubara, T. Ochi, T. Wakamiya, Z.-I. Yoshida, *J. Am. Chem. Soc.* **2008**, *130*, 13867–13869.

[10] For the sake of clarity and conciseness in the discussions, the kinetic data collected for **L1**, which bears electron-donating methoxy groups, are not further considered in Figure 1 and Table 1.

[11] Global quantum yields up to 64% have been reported for polynuclear Eu^{III} complexes, see K. Miyata, T. Ohba, A. Kobayashi, M. Kato, T. Nakanishi, K. Fushimi, Y. Hasegawa, *ChemPlusChem* **2012**, *77*, 277–280.

[12] $k_r^{Eu} = A(\Psi_J, \Psi_{J'}) = A_{MD,0} n^3 (I_{tot}/I_{MD})$ with $A_{MD,0} = 14.65\ s^{-1}$ for the magnetic dipolar $Eu(^5D_0 \rightarrow {}^7F_1)$ transition and a refractive index $n = 1.5$: A. Aebischer, F. Gumy, J.-C. G. Bünzli, *Phys. Chem. Chem. Phys.* **2009**, *11*, 1346–1353 and references therein.

[13] a) N. Sabbatini, M. Guardigli, I. Manet, *Handbook on the Physics and Chemistry of Rare Earths*, *Vol. 23* (Eds.: K. A. Gschneidner, Jr., L. Eyring), Elsevier Science, Amsterdam, **1996**, pp. 69–120; b) S. Faulkner, S. J. Pope, B. P. Burton-Pye, *Appl. Spectrosc. Rev.* **2005**, *40*, 1–35; c) M. D. Ward, *Coord. Chem. Rev.* **2010**, *254*, 2634–2642.

[14] a) S. Tobita, M. Arakawa, I. Tanaka, *J. Phys. Chem.* **1984**, *88*, 2697–2702; b) S. Tobita, M. Arakawa, I. Tanaka, *J. Phys. Chem.* **1985**, *89*, 5649–5654.

[15] D. Beljonne, Z. Shuai, G. Pourtois, J. L. Brédas, *J. Phys. Chem. A* **2001**, *105*, 3899–3907, and references therein.

[16] a) J. Jortner, M. Bixon, *Adv. Chem. Phys.* **1999**, *106*, 35–202; b) J. L. Brédas, D. Beljonne, V. Coropceanu, J. Cornil, *Chem. Rev.* **2004**, *104*, 4971–5003; c) K. Schmidt, S. Brovelli, V. Coropceanu, D. Beljonne, J. Cornil, C. Bazzini, T. Caronna, R. Tubino, F. Meinardi, Z. Shuai, J. L. Brédas, *J. Chem. Phys. A* **2007**, *111*, 10490–10499.

[17] A. Monguzzi, R. Tubino, S. Hoseinkhani, M. Campione, F. Meinardi, *Phys. Chem. Chem. Phys.* **2012**, *14*, 4322–4332.

[18] For intersystem crossing, solvent effects are expected to be small and are not considered in the determination of λ. As a first approximation, $\lambda = 1500$–$2000\ cm^{-1}$ are realistic values for polyaromatic scaffolds.[15,16]

[19] F. J. Steemers, W. Verboom, D. N. Reinhoudt, E. B. van der Tol, J. W. Verhoeven, *J. Am. Chem. Soc.* **1995**, *117*, 9408–9414.

Angewandte Chemie
Eine Zeitschrift der Gesellschaft Deutscher Chemiker

Supporting Information

69451 Weinheim, Germany

Perfluorinated Aromatic Spacers for Sensitizing Europium(III) Centers in Dinuclear Oligomers: Better than the Best by Chemical Design?**

Jean-François Lemonnier, Lucille Babel, Laure Guénée, Prasun Mukherjee, David H. Waldeck, Svetlana V. Eliseeva, Stéphane Petoud,* and Claude Piguet**

ange_201205082_sm_miscellaneous_information.pdf

Experimental Section

Chemicals were purchased from Strem, Acros, Fluka AG, and Aldrich, and used without further purification unless otherwise stated. Compound **1** was obtained from a literature procedure.[7] The lanthanide hexafluoroacetylacetonates [Ln(hfac)$_3$(diglyme)] were prepared from the corresponding oxide (Aldrich, 99.99%).[S1] Acetonitrile and dichloromethane were distilled over calcium hydride. Silica gel plates Merck 60 F_{254} were used for thin layer chromatography (TLC) and Fluka silica gel 60 (0.04-0.063 mm) or Acros neutral activated alumina (0.050-0.200 mm) was used for preparative column chromatography.

Preparation of 2. Pinalcodiboron ester (2.7 g, 10.6 mmol) and potassium acetate (1 g, 10 mmol) in degassed dioxane (40 mL) were added dropwise for 10 h to **1** (1.6 g, 3.6 mmol) and Pd(dppf)Cl_2 (150 mg, 0.18 mmol) in degassed dioxane (30 mL). The red solution was heated at 60°C during 4 days, during which the color slowly turned brown, then black. Aq. sat. NaCl solution (200 mL) was added and the resulting mixture was extracted with dichloromethane (4x200 mL). The dark organic phase was dried (Na_2SO_4) filtered and evaporated to dryness. The crude black oil was purified by column chromatography (Silicagel, CH_2Cl_2:CH_3OH = 100:0→98:2) to give **2** as an orange oil (1.44 g, 2.9 mmol, yield 80 %). ESI-MS (positive mode/CH_3OH): *m/z* 494.3 ([**2**+H]$^+$). ^{1}H NMR (400 MHz, $CDCl_3$): δ (ppm) 1.31 (t, ^3J=7.0 Hz, 3H), 1.32 (t, ^3J=7.0 Hz, 3H), 1.35 (s, 12H), 4.75 (q, ^3J=7.0 Hz, 4H), 7.31 (m, 2H), 7.43 (d, ^3J=9.0 Hz, 1H), 7.44(d, ^3J=7.9 Hz, 1H), 7.80 (d, ^3J=7.9 Hz, 1H), 7.85 (d, ^3J=9.0 Hz, 1H), 8.00 (t, ^3J=7.9 Hz, 1H), 8.33 (d, ^3J=7.9 Hz, 2H), 8.36 (s, 1H). ^{13}C NMR (101 MHz, $CDCl_3$) δ (ppm) 150.15, 149.94, 149.79, 142.86, 142.68, 138.20, 138.02, 135.91, 129.63, 127.67, 125.77, 125.65, 123.48, 122.71, 120.26, 110.22, 109.59, 83.65, 39.74, 24.86, 15.36.

Preparation of L4. Compound **2** (1.44 g, 2.6 mmol) in freshly distilled degassed dioxane (10 mL) was added dropwise for 4 h to CsF (0.9 g, 5.9 mmol), 1,4-dibromo-2,3,5,6-tetrafluorobenzene (370 mg, 1.2 mmol) and Pd(PPh_3)$_4$ (0.24 mmol, 270 mg) in freshly distilled degassed dioxane (5 mL). During the addition, the reacting mixture was stepwise heated to reflux and the color evolved from yellow to orange, brown and finally black. Aq. half-sat. Na_2CO_3 (200 mL) was added and the cooled mixture was extracted with dichloromethane (3x200 mL). The organic phase was washed with aq. half-sat. Na_2CO_3 (200 mL), dried (Na_2SO_4), filtered and evaporated to dryness. The crude brown oil was purified by column chromatography (Silicagel, CH_2Cl_2:CH_3OH = 100:0→97:3) and yielded a brown solid, which was dissolved in hot ethanol and precipitated with water to give **L4** as a pale yellow solid (440 mg, 0.49 mmol, yield 40%). ESI-MS (positive mode/CH_3OH): *m/z* 881.0 ([**L4**+H]$^+$), 1761.0 ([2**L4**+H]$^+$). ^{1}H NMR (400 MHz, $CDCl_3$): δ (ppm) 1.39 (t, ^3J=7.2 Hz, 3H), 1.42 (t, ^3J=7.2 Hz, 3H), 4.81 (q, ^3J=7.2 Hz, 2H), 4.85 (q, ^3J=7.2 Hz, 2H), 7.37 (m, 2H), 7.50 (d, ^3J=8.0

Hz, 1H), 7.54 (d, ^3J=8.3 Hz, 1H), 7.63 (d, ^3J=8.3 Hz, 1H), 7.89 (d, ^3J=7.2 Hz, 1H), 8.08 (t, ^3J=7.9 Hz, 1H), 8.08 (s, 1H), 8.37 (d, ^3J=7.9 Hz, 1H), 8.39 (d, ^3J=7.9 Hz, 1H). Elemental Analysis: calcd for $C_{52}H_{40}N_{10}F_4 \cdot 0.66H_2O$ C 69.94% H 4.66% N 15.68%, found C 69.94% H 4.61% N 15.63%.

Preparation of the complexes $[Ln_2(L4)(hfac)_6]$ (Ln = Gd, Eu). [Ln(hfac)$_3$(diglyme)] (0.025 mmol) was dissolved in chloroform (1 mL) and added to **L4** (11 mg, 0.025 mmol) in chloroform (1 mL). Precipitation occurred immediately and the complexes were collected as white off microcrystalline powders by filtration and dried under vacuum at 70 °C (yield = 80 %). Elemental Analysis: calcd for $[Eu_2(C_5F_6O_2H)_6(C_{52}H_{40}N_{10}F_4)]$ C 40.58% H 1.91% N 5.77, found C 40.34% H 1.96% N 5.71%. Calcd for $[Gd_2(C_5F_6O_2H)_6(C_{52}H_{40}N_{10}F_4)]$ C 40.40% H 1.90% N 5.74%, found C 40.42% H 2.07% N 5.60%. Monocrystals suitable for X-Ray diffraction were obtained by reacting 0.025 mmol of [Ln(hfac)$_3$(diglyme)] in acetonitrile (1 mL) with 0.0125 mmol of ligand in chloroform (1 mL). Slow evaporation yielded white prisms.

Spectroscopic measurements: ^{1}H, ^{19}F and ^{13}C NMR spectra were recorded at 298 K on *Bruker Avance* 400 MHz and *Bruker* DRX-300 MHz spectrometers. Chemical shifts are given in ppm with respect to TMS. Pneumatically-assisted electrospray (ESI-MS) mass spectra were recorded from 10^{-4} M solutions on an Applied Biosystems API 150EX LC/MS System equipped with a Turbo Ionspray source®. Elemental analyses were performed by K. L. Buchwalder from the Microchemical Laboratory of the University of Geneva. Electronic absorption spectra in the UV-Vis were recorded at 20 °C from solutions in CH_2Cl_2 with a Perkin-Elmer Lambda 900 spectrometer using quartz cells of 10 or 1 mm path length. Some of the excitation and emission spectra were recorded on a Perkin-Elmer LS-50B spectrometer equipped for low-temperature measurements And the other with a Jobin Yvon–Horiba Fluorolog-322 spectrofluorimeter equipped with a Hamamatsu R928 photomultiplier tube. Spectra were corrected for both excitation and emission responses (excitation lamp, detector and both excitation and emission monochromator responses). Quartz tube sample holders were employed. The quantum yields Φ for the free ligands in solution have been recorded through the relative method with respect to quinine sulfate 6.42 10^{-6} M in 0.05 M H_2SO_4 (refractive index 1.338 and quantum yield 0.546),[S2] and calculated using the equation

$$\frac{\Phi_x}{\Phi_r} = \frac{A_r(\tilde{\nu}) I_r(\tilde{\nu}) n_x^2 D_x}{A_x(\tilde{\nu}) I_x(\tilde{\nu}) n_r^2 D_r},$$

where x refers to the sample and r to the reference; A is the absorbance, ν the excitation wavenumber used, I the intensity of the excitation light at this energy, n the refractive index and D the integrated emission intensity

Quantum yield measurements of the solid state samples were measured on quartz tubes with the help an integration sphere developed by Frédéric Gumy and Jean-Claude G. Bünzli (Laboratory of Lanthanide Supramolecular Chemistry, École Polytechnique Féderale de Lausanne (EPFL), BCH 1402, CH-1015 Lausanne, Switzerland) commercialized by GMP S.A. (Renens, Switzerland)**.** Long luminescence lifetimes: triplet states (on Eu^{3+} and Gd^{3+} complexes) and lanthanide-centered luminescence lifetimes were measured at 293K using either a Nd:YAG Quantel YG 980 (354 nm, third harmonic) as the excitation source. Emission was collected at a right angle to the excitation beam and wavelengths were selected with interference filters. The signal was monitored by a Hamamatsu R928 photomultiplier tube, and was collected on a 500 MHz band pass digital oscilloscope (Tektronix TDS 724C). Experimental luminescence decay curves were treated with Origin 8.0 software using exponential fitting models. Three decay curves were collected on each sample, and reported lifetimes are an average of at least two successful independent measurements.
Rapid decays analysis (singlet states). The time-resolved luminescence decay kinetics was measured using the time-correlated single-photon counting (TCSPC) technique. Samples were excited with the frequency-doubled output (centered at ~330 nm) of a synchronously pumped cavity dumped dye laser (Coherent, Santa Clara, CA, model 599) using 4-(dicyanomethylene)-2-methyl-6-(4-dimethylaminostyryl)-4H-pyran (DCM) as the gain medium; emission from the sample was collected at different wavelengths using a monochromator. The instrument response function had a full-width-at-half-maximum (fwhm) of ~50 ps. A 1 cm path length quartz cuvette was used for all the time-resolved measurements in solutions. Measurements with solid samples were performed in a quartz capillary. All measurements were performed at room temperature. Experiments were performed with a 1MHz laser repetition rate. Lifetime decay traces were fitted by an iterative reconvolution method with IBH DAS 6 decay analysis software. Note that the short lifetimes observed for the L-Gd complexes may be limited by the instrument resolution.

X-Ray Crystallography. Summary of crystal data, intensity measurements and structure refinements for $[Eu_2(\mathbf{L4})(hfac)_6]$ are given in Table S1. The crystal was mounted on quartz fibers with protection oil. Cell dimensions and intensities were measured at 180 K on a Agilent Supernova diffractometer with graphite-monochromated Cu[Kα] radiation (λ = 1.54187 Å) and CCD camera. Data were corrected for Lorentz and polarization effects and for absorption. The structures were solved by direct methods (SIR97),[S3] all other calculation were performed with Shelx1[S4] systems and ORTEP[S5] programs. CCDC-874682 contains the supplementary crystallographic data. The cif files can be obtained free of charge via www.ccdc.cam.ac.uk/conts/retrieving.html (or from the Cambridge Crystallographic Data Centre, 12 Union Road, Cambridge CB2 1EZ, UK; fax: (+ 44) 1223-336-033; or deposit@ccdc.cam.ac.uk).

References

[S1] (a) W. J. Evans, D. G. Giarikos, M. A. Johnston, M. A. Greci, J. W. Ziller, *J. Chem. Soc. Dalton Trans.*, **2002**, 520-526. (b) G. Malandrino, R. Lo Nigro, I. L. Fragalà, C. Benelli, *Eur. J. Inorg. Chem.*, **2004**, 500-509.

[S2] S. R. Meech, D. C. Phillips, *J. Photochem.* **1983**, *23*, 193-217.

[S3] A. Altomare, M. C. Burla, M. Camalli, G. Cascarano, C. Giacovazzo, A. Guagliardi, G. Moliterni, G. Polidori, R. Spagna, *J. Appl. Cryst.* **1999**, *32*, 115-119.

[S4] G. M. Sheldrick, SHELXL97 *Program for the Solution and Refinement of Crystal Structures*, University of Göttingen, Germany, 1997.

[S5] *ORTEP3* L. J. Farrugia, *J. Appl. Crystallogr.* **1997**, *30*, 565.

Table S1 Summary of Crystal Data, Intensity Measurements and Structure Refinements for $[Eu_2(\mathbf{L4})(hfac)_6]$.

	$[Eu_2(\mathbf{L4})(hfac)_6]$
Empirical formula	$C_{82}H_{46}Eu_2F_{40}N_{10}O_{12}$
Formula weight	2427.21
Temperature	180(2) K
Wavelength	1.54184 Å
Crystal System, Space group	Triclinic, *P*-1
Unit cell dimensions	a = 12.5477(3) Å
	b = 12.7655(4) Å
	c = 14.4370(4) Å
	α = 93.650(2)°
	β = 102.812(2)°
	γ = 102.714(2)°
Volume in Å^3	2184.20(11) Å^3
Z, Calculated density	1, 1.845 Mg/m^3
Absorption coefficient	11.569 mm^{-1}
F(000)	1190
Theta range for data collection	3.16 to 73.43 °
Limiting indices	-12<=h<=15,
	-15<=k<=15,
	-17<=l<=17
Reflections collected / unique	24859 / 8583
	[R(int) = 0.0362]
Completeness to theta	66.97° / 99.9%
Data / restraints / parameters	8583 / 0 / 660
Goodness-of-fit on F^2	1.156
Final R indices [I>2σ(I)]	R_1 = 0.0341,
	ωR_2 = 0.0900
R indices (all data)	R_1 = 0.0371,
	ωR_2 = 0.0927
Largest diff. peak and hole	0.759 and -0.745 e.Å^{-3}

Table S2 Selected Bond Distances (Å), Bond Angles (°) in $[Eu_2(\mathbf{L4})(hfac)_6]$.

Bond distances (Å)

Atom 1	Atom 2	Distance	Atom 1	Atom 2	Distance
Eu(1)	O(1)	2.387(2)	Eu(1)	N(1)	2.547(2)
Eu(1)	O(2)	2.466(2)	Eu(1)	N(4)	2.535(3)
Eu(1)	O(6)	2.430(2)	Eu(1)	O(5)	2.491(2)
Eu(1)	O(4)	2.396(2)	Eu(1)	N(3)	2.626(2)
Eu(1)	O(3)	2.398(2)	Eu(1)	Eu(1)’	14.667(1)

Symmetry operation (’) -*x*,1-*y*,1-*z*.

Angles (°)

At. 1	At. 2	At. 3	angle	At. 1	At. 2	At. 3	angle
O(1)	Eu(1)	O(2)	69.17(8)	O(4)	Eu(1)	N(4)	84.42(8)
O(1)	Eu(1)	O(6)	144.60(8)	O(3)	Eu(1)	N(4)	140.85(8)
O(2)	Eu(1)	O(6)	131.04(8)	N(1)	Eu(1)	N(4)	125.99(8)
O(1)	Eu(1)	O(4)	135.90(8)	O(1)	Eu(1)	O(5)	127.59(8)
O(2)	Eu(1)	O(4)	69.34(8)	O(2)	Eu(1)	O(5)	127.48(8)
O(6)	Eu(1)	O(4)	77.00(8)	O(6)	Eu(1)	O(5)	67.96(8)
O(1)	Eu(1)	O(3)	78.19(8)	O(4)	Eu(1)	O(5)	70.64(7)
O(2)	Eu(1)	O(3)	69.87(8)	O(3)	Eu(1)	O(5)	67.53(8)
O(6)	Eu(1)	O(3)	132.76(8)	N(1)	Eu(1)	O(5)	72.33(8)
O(4)	Eu(1)	O(3)	74.17(8)	N(4)	Eu(1)	O(5)	134.93(8)
O(1)	Eu(1)	N(1)	68.20(8)	O(1)	Eu(1)	N(3)	73.10(8)
O(2)	Eu(1)	N(1)	135.19(9)	O(2)	Eu(1)	N(3)	116.11(8)
O(6)	Eu(1)	N(1)	92.65(8)	O(6)	Eu(1)	N(3)	71.64(8)
O(4)	Eu(1)	N(1)	142.78(8)	O(4)	Eu(1)	N(3)	140.78(8)
O(3)	Eu(1)	N(1)	88.45(8)	O(3)	Eu(1)	N(3)	145.05(8)
O(1)	Eu(1)	N(4)	96.53(9)	N(1)	Eu(1)	N(3)	62.70(8)
O(2)	Eu(1)	N(4)	72.03(8)	N(4)	Eu(1)	N(3)	63.29(8)
O(6)	Eu(1)	N(4)	70.22(8)	O(5)	Eu(1)	N(3)	116.41(7)

Table S3 Selected Least-Squares Planes Data for in $[Eu_2(\mathbf{L4})(hfac)_6]$.

Least-Squares Planes

Least-squares planes description	Abbreviation	Max. deviation/Å	Atom
Benzimidazole 1	Bz1		
C1 C2 C3 C4 C5 C6 N2 C7 N1		0.038(1)	C7
Pyridine	Py		
N3 C10 C11 C12 C13 C14		0.011(1)	C13
Benzimidazole 3	Bz3		
C15 N5 C16 C17 C18 C19 C20 C21 N4		0.029(1)	N4
Phenyl	Ph		
C24 C25 C26 C24' C25' C26'		0.000	

Interplanar angles (°)

	Bz1	Py	Bz3	Ph
Bz1		10.85(3)	21.96(2)	76.35(7)
Py			20.36(3)	83.02(9)
Bz3				66.2(1)
Ph				

Table S4 Bond Distances ($\delta_{Eu,j}$), Bond Valences （$\nu_{Eu,j}$)[a] and Total Atom Valence (V_{Eu})[b] in the Crystal Structure of [Eu_2(**L4**)(hfac)$_6$].

Atom	Donor type	$\delta_{Eu,j}$ / Å	$\nu_{Eu,j}$	
O1	hfac	2.387	0.389	
O2	hfac	2.466	0.315	
O3	hfac	2.398	0.378	
O4	hfac	2.396	0.380	
O5	hfac	2.491	0.294	Average O-hfac
O6	hfac	2.430	0.347	0.35(4)
N1	bzim	2.547	0.350	
N3	py	2.626	0.285	Average N-heterocyclic
N4	bzim	2.535	0.364	0.33(4)
		V_{Eu}	3.102	

[a] $\nu_{Ln,j} = e^{\left[\left(R_{Ln,j}-\delta_{Ln,j}\right)/b\right]}$, whereby $\delta_{Ln,j}$ is the Ln-donor atom *j* distance with *b* = 0.37Å ((a) Brown, I. D.; Altermatt, D. *Acta Cryst B* **1985**, *41*, 244-247. (b) N. E. Breese, M. O'Keeffe, *Acta Cryst. B* **1991**, *47*, 192-197. (c) I. D. Brown, *Acta Cryst B* **1992**, *48*, 553-572. (d) I. D. Brown, *The Chemical Bond in Inorganic Chemistry*, Oxford University Press, Oxford, **2002**. (e) I. D. Brown, *Chem. Rev.* **2009**, *109*, 6858-6919). The valence bond parameters $R_{Ln,N}$ and $R_{Ln,O}$ are taken from A. Trzesowska, R. Kruszynski, T. J. Bartczak, *Acta Cryst B* **2004**, *60*, 174-178 and A. Trzesowska, R. Kruszynski, T. J. Bartczak, *Acta Cryst B* **2005**, *61*, 429-434. [b] $V_{Eu} = \sum_j \nu_{Eu,j}$.

Table S5 Ln···Ln, Ln-N and Ln-O Distances (Å), Bond Valences ($\nu_{Ln,j}$) and Bond Valence Sums (V_{Ln}) in the Crystal Structures of $[Yb_2(\mathbf{L2})(hfac)_6]$, $[Yb_2(\mathbf{L3})(hfac)_6]$ and $[Eu_2(\mathbf{L4})(hfac)_6]$.[a]

	$[Yb_2(\mathbf{L2})(hfac)_6]$	$[Yb_2(\mathbf{L3})(hfac)_6]$	$[Eu_2(\mathbf{L4})(hfac)_6]$
Ln-N_{bzim} [b] /Å	2.443(4)	2.476(4)	2.541(9)
Ln-N_{py} /Å	2.519	2.526	2.626
Ln-O [c] /Å	2.38(8)	2.36(7)	2.43(4)
Ln···Ln /Å	12.624	14.77	14.668
$\nu_{Ln,N(bzim)}$ [b]	0.359(4)	0.328(4)	0.358(8)
$\nu_{Ln,N(py)}$	0.292	0.287	0.285
$\nu_{Ln,O}$ [c]	0.33(6)	0.34(6)	0.35(4)
V_{Ln}	2.964	2.980	3.102
Reference	7	7	This work

[a] See Table S4 for the definitions of $\nu_{Ln,j}$ and V_{Ln}. [b], [c] Each value is the average of two[b] or six[c] bond distances and the numbers between brackets correspond to the standard deviations affecting the average values (the original uncertainties affecting each bond length are given in Tables S4; bzim = benzimidazole and py = pyridine).

Table S6. Ligand-centered Absorption and Emission Properties of **L2-L4** and of their Complexes $[Gd_2(\mathbf{L}\boldsymbol{k})(hfac)_6]$.

Compound	*T* /K	$\lambda_{max,abs}$ /cm^{-1} [a] $^1\pi\rightarrow{}^1\pi^*$	$\lambda_{max,flu}$ /cm^{-1} $^1\pi^*\rightarrow{}^1\pi$	Lifetime /ns τ ($^1\pi^*$)	$\lambda_{max,phos}$ /cm^{-1} $^3\pi^*$	Lifetime /ms τ ($^3\pi^*$)	Reference
Solution (CH_2Cl_2)							
L2	293	34250(57000)/ 29850(69500)	23900/ 24650	2.04(7)	20200	[b]	[7]
L3	293	37480(43400)/ 29860(73300)	25400/ 25500	1.374(4)	20240	[b]	[7]
L4	293	37300(59000)/ 30400(87000)	25600/ 24400	1.05(3)	20800	[b]	This work
Solid state							
L2	293	29850	23350	0.149(12)	-	-	[7]
	77	-	23310	-	18720	[b]	
L3	293	29660	24180	0.160(3)	-	-	[7]
	77	-	25250	-	19480	[b]	
L4	293	30300	24400	0.25(2)	-	-	This work
	77	-	25700	-	21000	[b]	
$[Gd_2(\mathbf{L2})(hfac)_6]$	293	28650	22620	0.060(2)	19070	0.123(7)	[7]
	77	-	22600		19070	0.69(5)	
$[Gd_2(\mathbf{L3})(hfac)_6]$	293	28650	23820	0.066(14)	19470	0.16(2)	[7]
	77	-	22700	-	19470	0.67(5)	
$[Gd_2(\mathbf{L4})(hfac)_6]$	293	30300	23260	0.029(6)	20300	0.11(3)	This work
	77	-	25500	-	20300	1.70(5)	

[a] The molar absorption coefficients ε are given between parentheses in $M^{-1}\cdot cm^{-1}$. [b] The intensity is too weak to obtain reliable lifetime measurements.

Table S7. Fluorescence Quantum Yields ($\Phi_L^L\left(^1\pi^*\right)$) and Lifetimes ($\tau_L(^1\pi^*)$), Computed Rate Constants (k_r^F, k_{nr}^F and k_{ISC}) and π-Conjugation Lengths (A_π) for **L2-L4** and for their Complexes [Gd_2(**L*k***)(hfac)$_6$] at 293K.

Compound	Conc./ M	$\bar{\nu}_{exc}$ /cm^{-1}	$\varepsilon(\bar{\nu}_{exc})$ /M^{-1}cm^{-1}	$\Phi_L^L\left(^1\pi^*\right)$	$\tau_L(^1\pi^*)$/ ns	k_r^F /ns^{-1}	$k_{nr}^F + k_{ISC}$ /ns^{-1}	k_{ISC} [a] /ns^{-1}	η_{ISC} [a]	k_{nr}^F [b] /ns^{-1}	A_π
Solution (CH_2Cl_2)											
QSO_4 [c]	$6.42\cdot10^{-6}$	27780	8100	0.546	-	-	-	-	-	-	0.18
L2	10^{-5}	27780	4000	0.80(8)	2.04(7)	0.39(4)	0.10(7)	-	-	-	1.39(6)
L3	10^{-5}	27780	4300	0.74(8)	1.374(4)	0.54(6)	0.17(2)	-	-	-	1.05(7)
L4	10^{-6}	28650	7980	0.69(8)	1.05(3)	0.66(8)	0.3(1)	-	-	-	0.80(7)
Solid state											
L2	-	29550	-	0.045(2)	0.149(12)	0.30(3)	6.41(4)	-	-	-	-3.05(3)
L3	-	29550	-	0.049(2)	0.160(3)	0.31(1)	5.94(2)	-	-	-	-2.97(3)
L4	-	28170	-	0.045(5)	0.25(2)	0.18(2)	3.82(4)	-	-	-	-3.06(7)
[Gd_2(**L2**)(hfac)$_6$]	-	29850	-	0.00316(7)	0.060(2)	0.053(2)	16.6(7)	10.0(6)	0.60(3)	6.7(8)	-4.84(5)
[Gd_2(**L3**)(hfac)$_6$]	-	29850	-	0.0035(5)	0.066(14)	0.05(1)	15(4)	9(2)	0.59(13)	6(4)	-4.8(3)
[Gd_2(**L4**)(hfac)$_6$]	-	28170	-	0.0037(2)	0.029(6)	0.13(1)	34(4)	30(4)	0.88(15)	4(5)	-3.4(6)

[a] k_{ISC} is estimated for [Gd_2(**L*k***)(hfac)$_6$] with eq. 6 and η_{ISC} with eq. 2 (see text). [b] $k_{nr}^F = \left(1/\tau_L\left(^1\pi^*\right)\right) - k_{ISC} - k_r^F$. [c] Quinine sulphate in H_2SO_4 0.05 M.[S2]

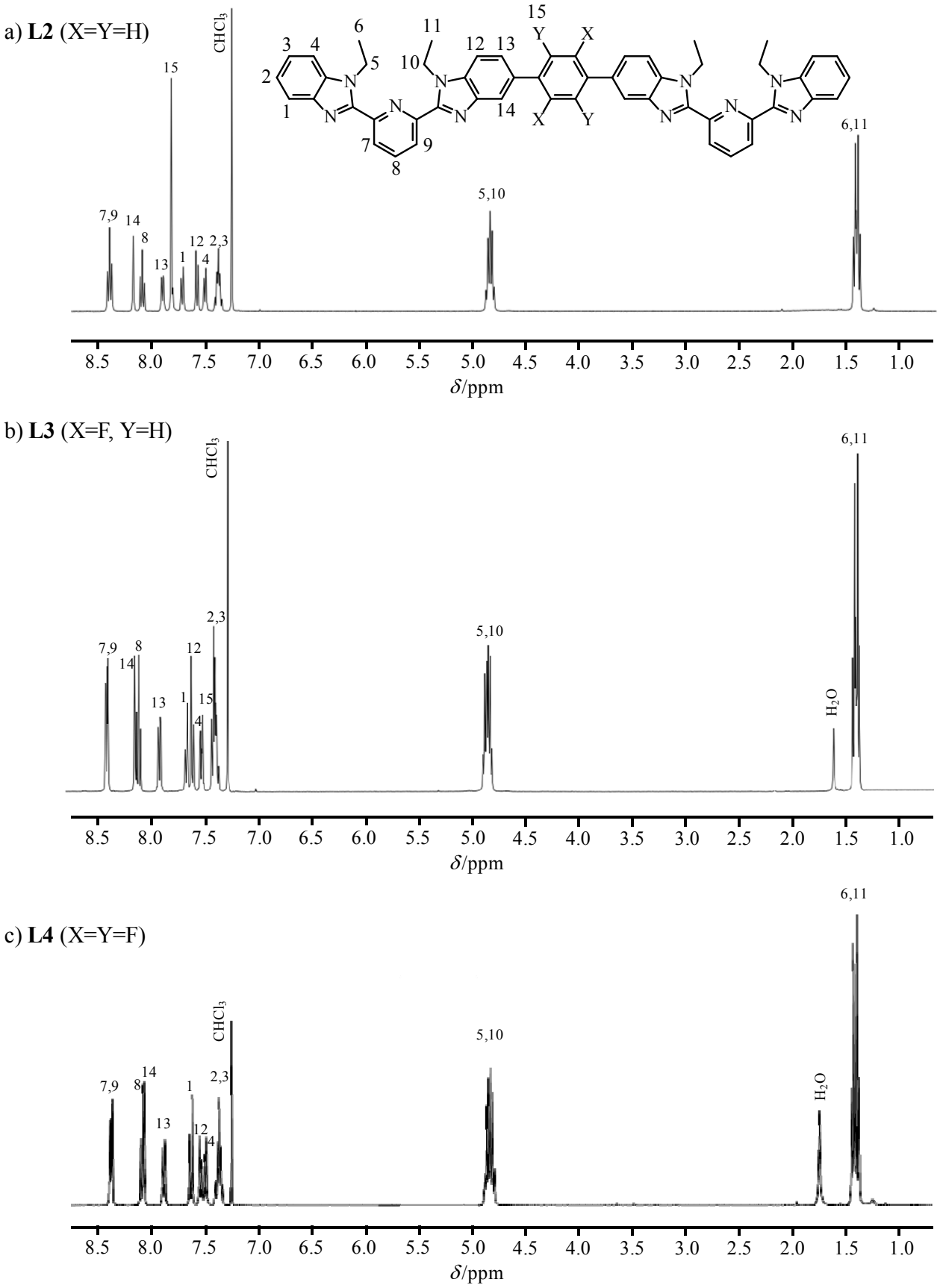

Figure S1 ^{1}H NMR spectra of the ligands **L2-L4** ($CDCl_3$, 293 K).

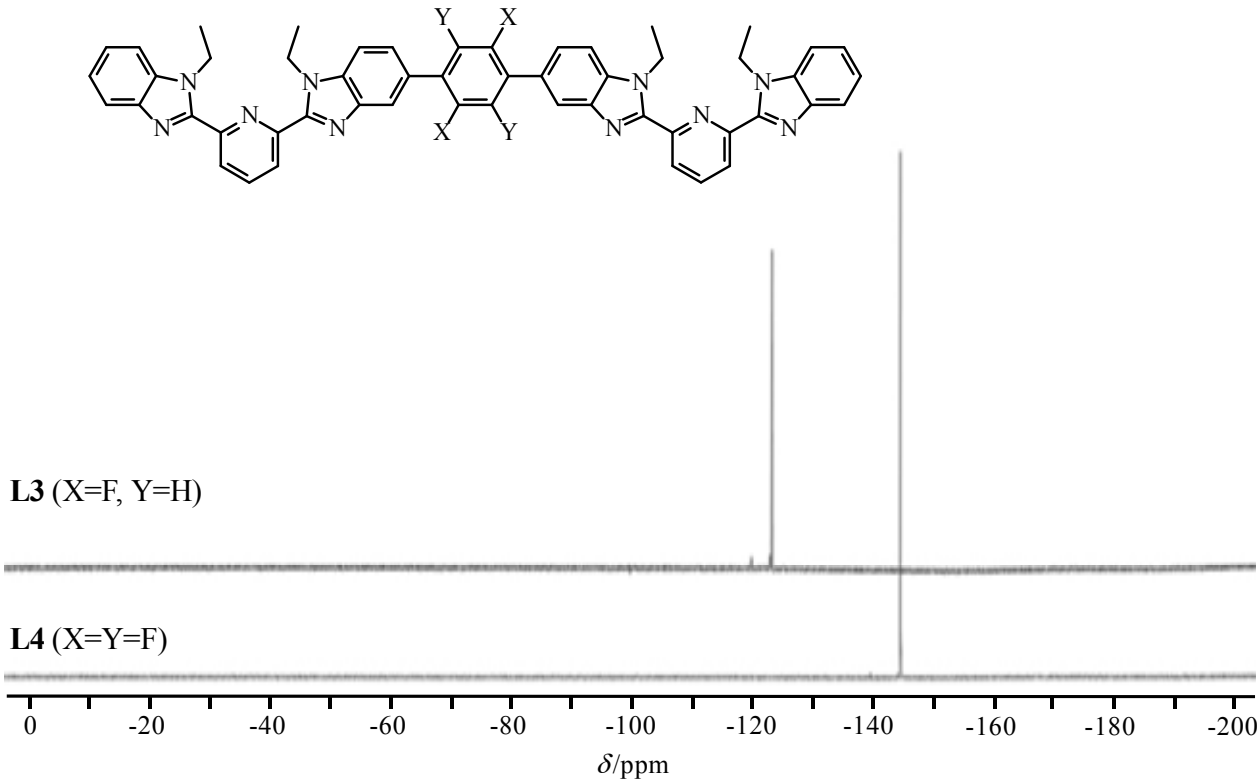

Figure S2 ^{19}F NMR spectra of the ligands **L3**-**L4** ($CDCl_3$, 293 K).

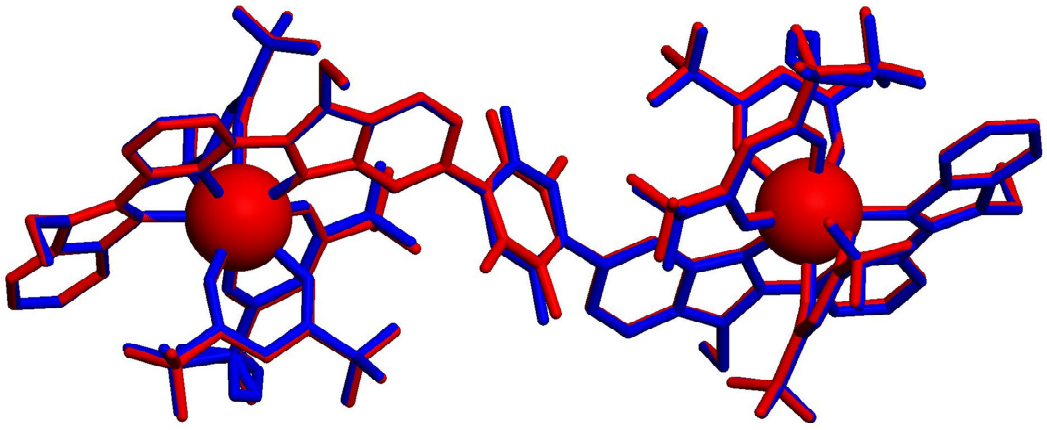

Figure S3 Superimposition of the molecular structures of $[Eu_2(\mathbf{L4})(hfac)_6]$ (red) and $[Yb_2(\mathbf{L3})(hfac)_6]$ (blue).[7]

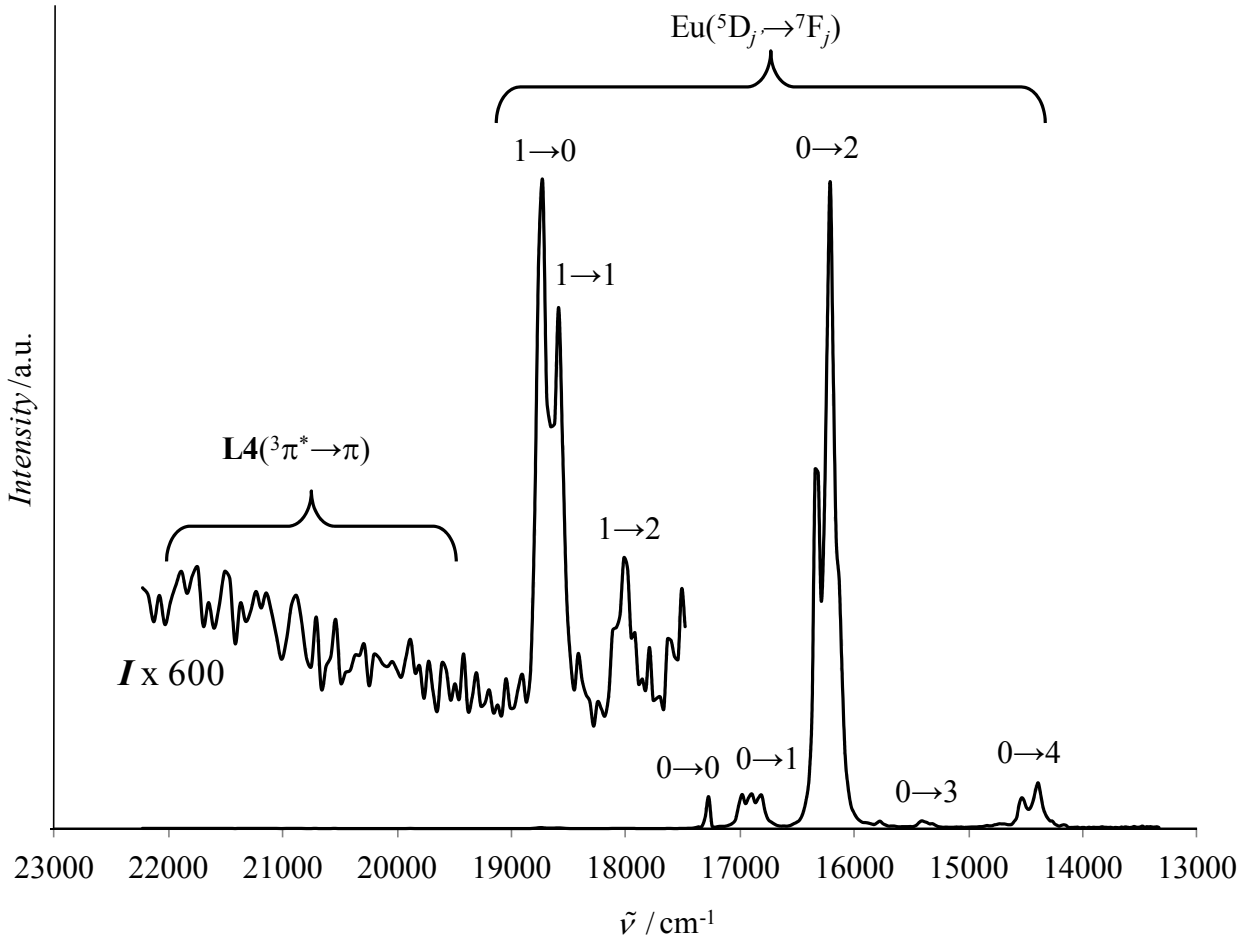

Figure S4 Emission spectrum of $[Eu_2(\mathbf{L4})(hfac)_6]$ (solid state, 293 K, $\tilde{\nu}_{exc}$ = 28200 cm^{-1}).

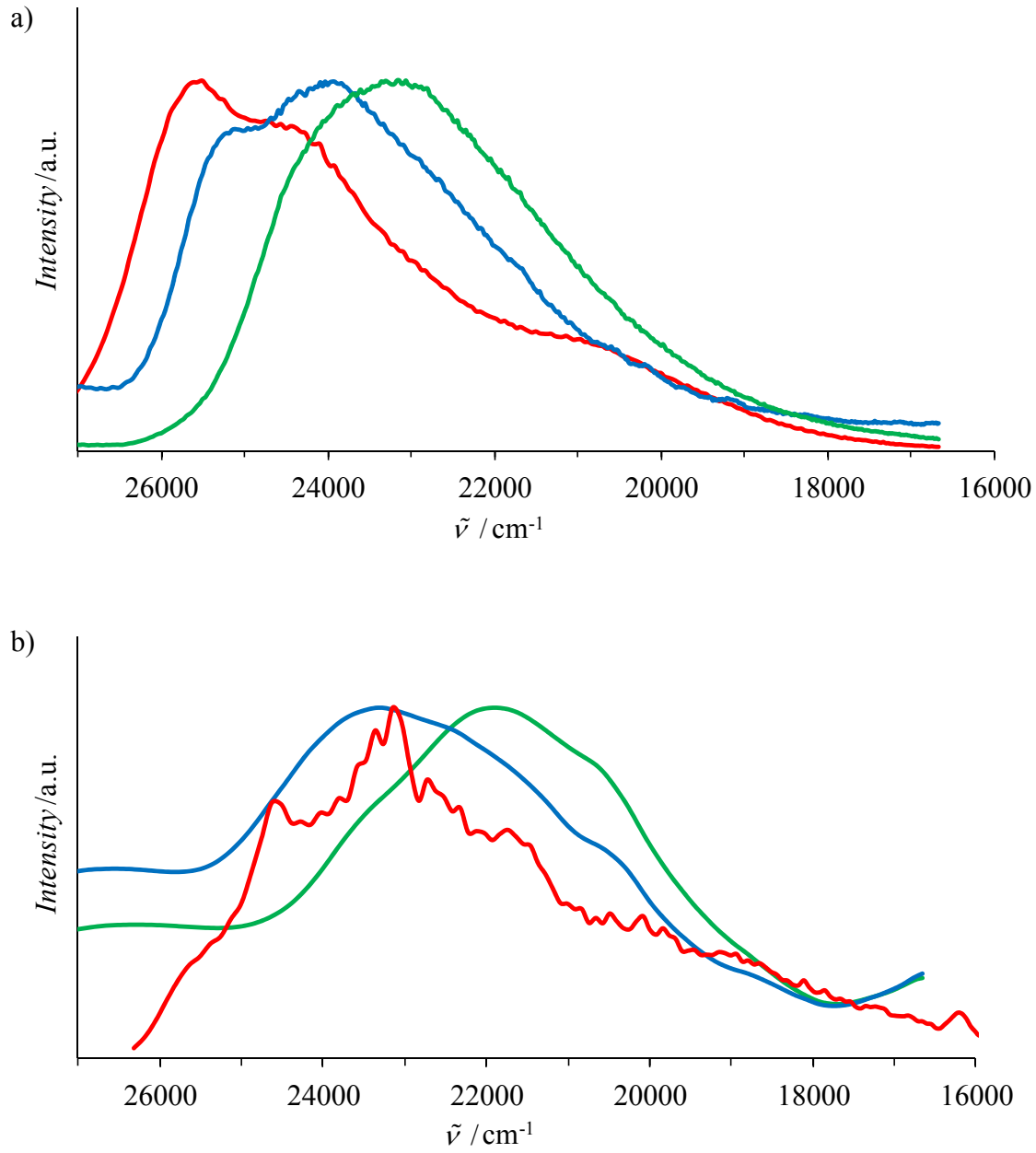

Figure S5 Emission spectra showing the ligand-centered $^1\pi^* \rightarrow {}^1\pi$ fluorescence in a) **L*k*** and b) $[Gd_2(\mathbf{L}k)(hfac)_6]$ (solid state, 77 K, $\tilde{\nu}_{exc}$ = 28200 cm^{-1}). Color code: **L2** = green, **L3** = blue, **L4** = red.

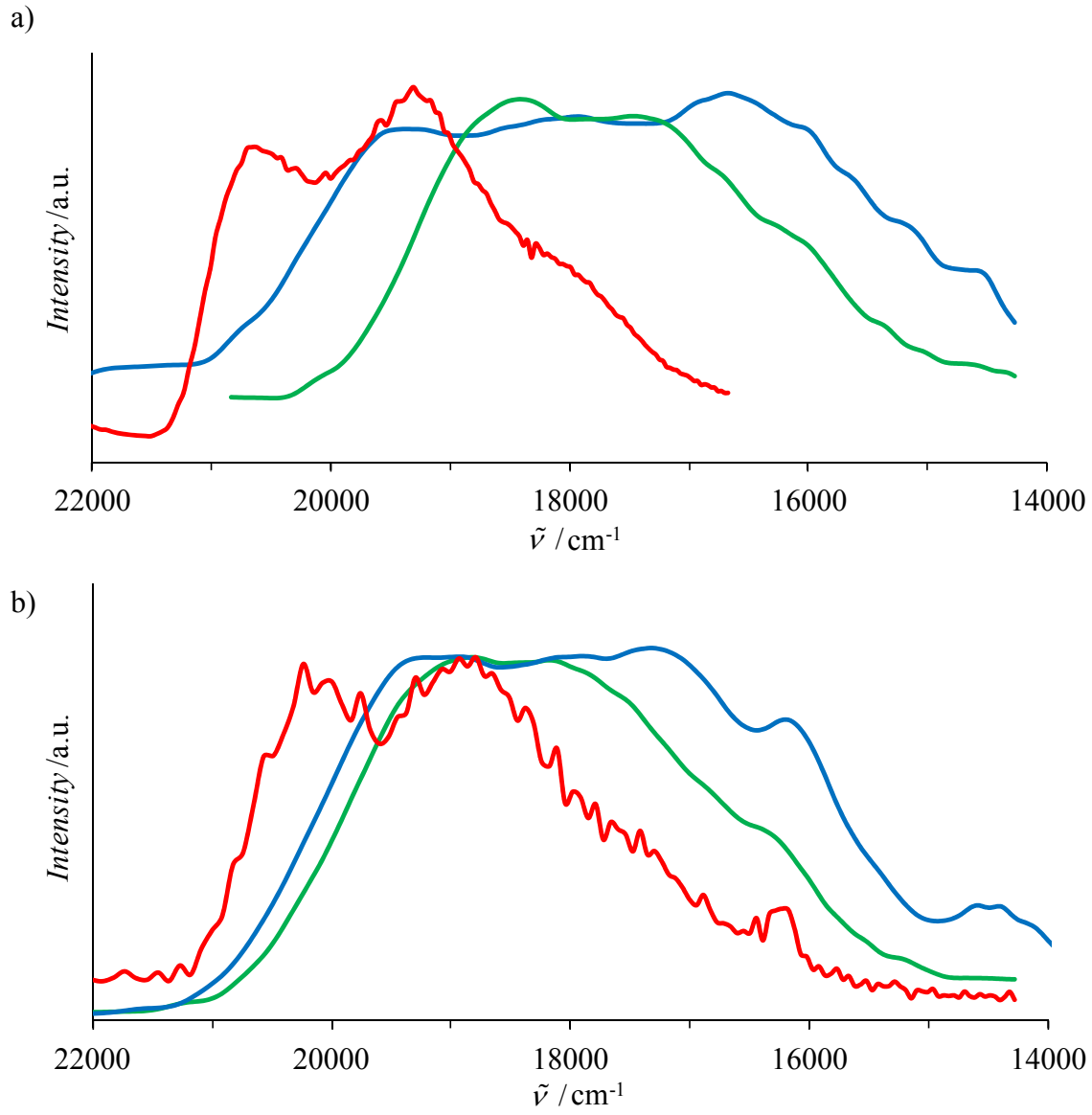

Figure S6 Emission spectra showing the ligand-centered $^3\pi^* \rightarrow {}^1\pi$ phosphorescence in a) **L*k*** and b) $[Gd_2(\mathbf{L}k)(hfac)_6]$ (solid state, 77 K, $\tilde{\nu}_{exc}$ = 28200 cm^{-1}, delay time 0.05 ms). Color code: **L2** = green, **L3** = blue, **L4** = red.

Appendix I: **Geometrical analysis of the Eu(III) coordination sphere in [Eu_2(L4)$(hfac)_6$]**

Eu(III) is nine-coordinated by the three nitrogen atoms of the tridentate aromatic of one binding unit in **L4** and by the six oxygen atoms of three didentate hexafluoroacetylacetonate anions. The donor atoms occupy the vertice of a highly distorted polyhedron, which is usually analyzed as a distorted monocapped square antiprism for ternary complexes [Ln(**L**)$(hfac)_3$], where **L** is a tridentate neutral ligand.[S6] When analogous geometries are to be compared, the use of the famous *S* angle of the 'shape measure' parameter is pertinent,[S7] but it is of limited interest for characterizing a single structure, and we therefore resort to the vectorial shape analysis proposed by leBorgne et al.[S8] Following this approach, the coordination sphere of Eu(III) can be described as a distorted monocapped square antiprism (MSA), in which O2, O4, O6, N4 and O1, O3, O5, N3 define, respectively, the lower and the upper tetragonal faces of the approximate antiprism, the latter being capped by N1 (Fig S7a). The computed resulting vector *R*1 (resp. *R*2) corresponds to the sum of the four Eu-donor atoms vectors forming the upper (resp. the lower) tetragonal face of the antiprism. The θ angles ($40.0 \leq 85.9°$, average 61(16)°) between each generating upper Eu-donor vector and *R*1 (resp between each lower Eu-donor vector and *R*2), measure the flatening of the antiprism along the pseudo-C_4 axis defined by the *R*1-*R*2 direction, whereas the ϕ angle (170.5°) between *R1* and *R*2 indicates a limited, but significant bending of the two tetragonal faces ($\phi = 180°$ in an ideal MSA, Table S8). The rather broad distribution of θ_i combined with the noticeable deviation of the capping N1 atom from the pseudo-C_4 axis ($\alpha = 25.8°$, Table S8 and Fig. S7a) suggest some severe distortions from the idealized Johnson capped square antiprism[S9] despite a rather regular distribution of the ω_i angles between the projected vectors of the tetrapodes along the pseudo-C_4 axis (intra-tetrapode = 90(15)°, ideal: 90° and inter-tetrapode = 45(14)°, ideal: 45°; Fig S7a right and Table S8). According that all Eu-O and Eu-N bonds are comparable, vector normalization to unit length[S8] does not significantly affect the geometrical analysis (Table S8). A more rigorous analysis of the coordination sphere of nine-coordinate metal complexes based on the spherical relaxation of the five Johnson polyhedra possessing nine vertices[S9] shows that the distorted coordination sphere in [Eu_2(**L4**)$(hfac)_6$] can be best described as a 2:5:2 hula hoop (HH), in which the basal plane is defined by N1, N3, N4, O3, O4 related by a five-fold pseudo-symmetry axis with two vertices (O5, O6) and (O1,O2), each related by a two-fold pseudo-symmetry axis, and located on each opposite side of the central pentagone (Fig. S7b).[S9] Only minor deviation from this ideal geometry is demonstrated by the $\delta = 169.4°$ and $\gamma = 177.9°$ angles measured between the directing vectors characterizing each didentate hfac anion (ideal 2:5:2 hula hoop: $\delta = \gamma = 180°$; Fig. S7c).

Table S8 Selected structural data for the lanthanide coordination spheres in $[Eu_2(\mathbf{L4})(hfac)_6]$.

			Angle ϕ [a] / °
	$[Eu_2(\mathbf{L4})(hfac)_6]$		Perfect MSA[b]
	Standard	Normalized	
R^1-Eu-R^2	170.5	167.1	180
			Angle α [a] / °
	$[Eu_2(\mathbf{L4})(hfac)_6]$		Perfect MSA[b]
	Standard	Normalized	0
	25.8	27.0	0
			Angles θ_t [a] / ° (distal tetrapodes)
	$[Eu_2(\mathbf{L4})(hfac)_6]$		Perfect MSA[b]
R^1-Eu-O1	51.7	51.3	ρ
R^1-Eu-O3	60.5	57.2	ρ
R^1-Eu-O5	76.8	76.6	ρ
R^1-Eu-N3	85.9	88.9	ρ
R^2-Eu-O2	63.9	64.2	ρ
R^2-Eu-O4	44.4	43.5	ρ
R^2-Eu-O6	67.1	66.9	ρ
R^2-Eu-N4	40.0	40.9	ρ
			Angles ω_{ij} [a] / °
	$[Eu_2(\mathbf{L4})(hfac)_6]$		Perfect MSA[b]
	Standard	Normalized	
Proj[O1]-Eu-Proj[O3][c]	92.9	93.9	90
Proj[O3]-Eu-Proj[O5]	71.9	71.8	90
Proj[O5]-Eu-Proj[N3]	120.3	120.0	90
Proj[N3]-Eu-Proj[O1]	75.0	74.5	90
Proj[O2]-Eu-Proj[O4]	82.7	81.5	90
Proj[O4]-Eu-Proj[O6]	97.5	98.5	90
Proj[O6]-Eu-Proj[N4]	90.7	92.3	90
Proj[N4]-Eu-Proj[O2]	89.2	87.7	90
Proj[O2]-Eu-Proj[O1]	40.0	40.1	45
Proj[O1]-Eu-Proj[N4]	49.2	47.7	45
Proj[N4]-Eu-Proj[N3]	25.8	27.5	45
Proj[N3]-Eu-Proj[O6]	64.8	64.8	45

Proj[O6]-Eu-Proj[O5]	55.5	55.3	45
Proj[O5]-Eu-Proj[O4]	42.1	43.5	45
Proj[O4]-Eu-Proj[O3]	29.8	28.3	45
Proj[O3]-Eu-Proj[O2]	52.9	52.8	45

[a] For the definition of ϕ, α, θ_i and ω_{ij}, see Fig. S7a. The error in the angles is typically 0.5°. [b] MSA = monocapped square antiprism. [c] Proj[O*i*] and Proj[N*i*] are the projections of O*i* and respectively N*i* along the R^2-R^1 direction onto a perpendicular plane passing through the lanthanide atom. R^1 = Eu-O1 + Eu-O3 + Eu-O5 + Eu-N3 and R^2 = Eu-O2 + Eu-O4 + Eu-O6 + Eu-N4.

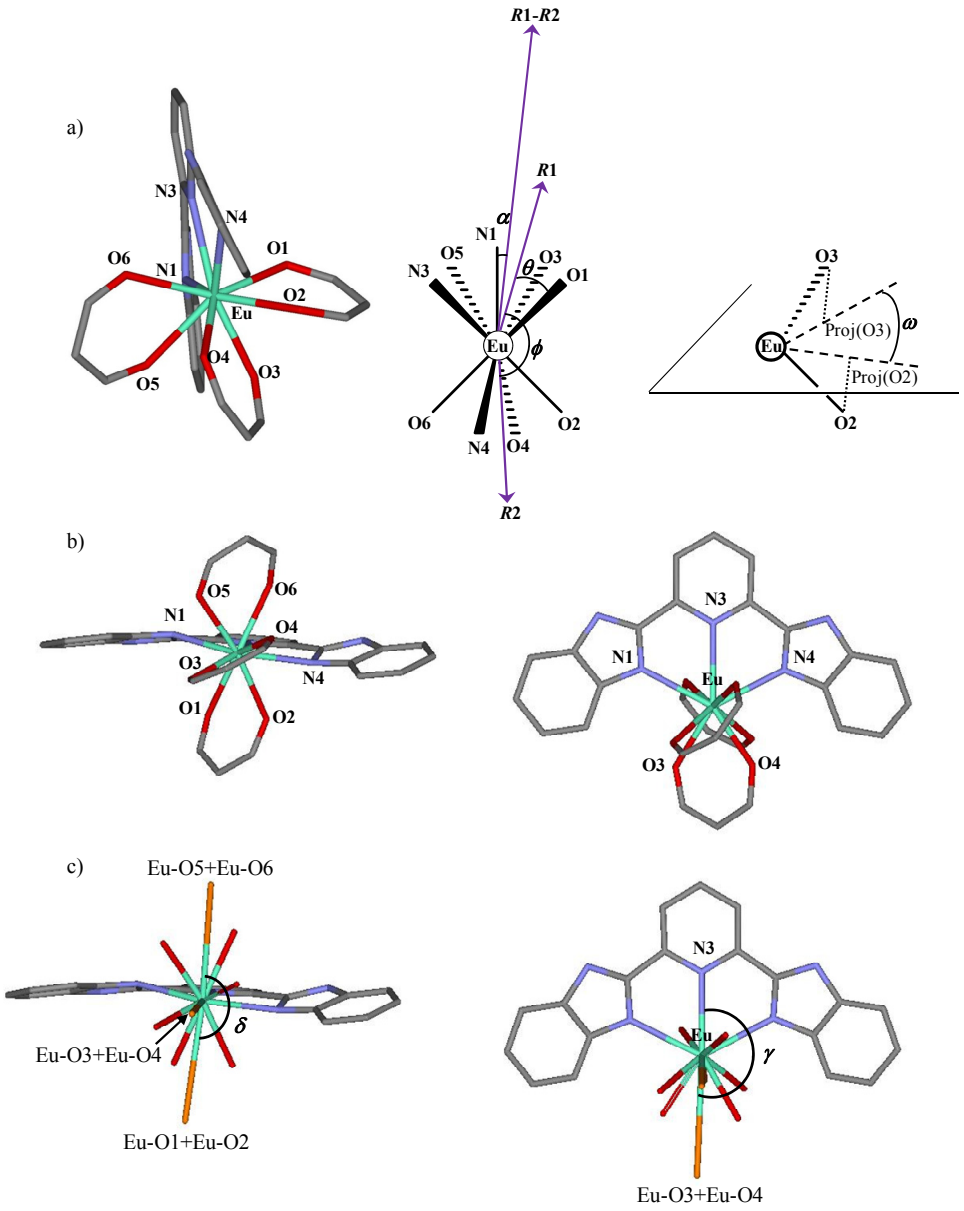

Figure S3 Geometrical analyses of the Eu(III) coordination sphere in [Eu_2(**L4**)$(hfac)_6$] as a) a standard distorted monocapped square antiprismatic polyhedron,[S8] b) and c) 2:5:2 hula hoop (HH).[S9]

References

[S6] Y. Kuramochi, T. Nakagawa, T. Yokoo, J. Yuasa, T. Kawai, Y. Hasegawa, *Dalton Trans.* **2012**, *41*, 6634-6640.

[S7] (a) B. E. Robertson, *Inorg. Chem.*, **1977**, *16*, 2735–2742. (b) M. C. Favas, D. L. Kepert, *Prog. Inorg. Chem.* **1981**, *28*, 309–367. (c) J. Xu, E. Radkov, M. Ziegler, K. N. Raymond, *Inorg. Chem.* **2000**, 39, 4156–4164. (d) S. V. Eliseeva, O. V. Kotova, F. Gumy, S. N. Semenov, V. G. Kessler, L. S. Lepnev, J.-C. G. Bünzli, N. P. Kuzmina, *J. Phys. Chem. A*, **2008**, *112*, 3614–3614. (e) T. Harada, Y. Nakano, M. Fujiki, M. Naito, T. Kawai, Y. Hasegawa, *Inorg. Chem.* **2009**, *48*, 11242–11250. (f) B. E. Robertson, *Inorg. Chem.*, **1977**, *16*, 2735–2742. (e) M. C. Favas, D. L. Kepert, *Prog. Inorg. Chem.* **1981**, *28*, 309–367.

[S8] T. Le Borgne, J.-M. Bénech, S. Floquet, G. Bernardinelli, C. Aliprandini, P. Bettens, C. Piguet, *Dalton Trans.* **2003**, 3856-3868.

[S9] A. Ruiz-Martinez, D. Casanova, S. Alvarez, *Chem. Eur. J.* **2008**, *14*, 1291-1303.